Materials and Design 66 (2015) 274–283

Contents lists available at ScienceDirect

Materials and Design

journal homepage: www.elsevier.com/locate/matdes

Low cycle fatigue of SiCp reinforced AA2009 composites

M.J. Luk [a], F.A. Mirza [a], D.L. Chen [a,*], D.R. Ni [b], B.L. Xiao [b], Z.Y. Ma [b,*]

[a] Department of Mechanical and Industrial Engineering, Ryerson University, 350 Victoria Street, Toronto, Ontario M5B 2K3, Canada
[b] Shenyang National Laboratory for Materials Science, Institute of Metal Research, Chinese Academy of Sciences, 72 Wenhua Road, Shenyang 110016, China

ARTICLE INFO

Article history:
Received 19 June 2014
Accepted 25 October 2014
Available online 4 November 2014

Keywords:
Metal-matrix composites
Low cycle fatigue
Cyclic deformation
Strain ratio
Mean stress

ABSTRACT

Strain-controlled low cycle fatigue (LCF) characteristics of an extruded Al–Cu–Mg aluminum alloy reinforced with SiC particles (SiCp/AA2009 composite) in the T4 and T6 heat treatment conditions were investigated. In comparison with the T6 condition with Al_2CuMg precipitates, the composite in the T4 condition had a higher ductility and equivalent ultimate tensile strength despite a lower yield strength, leading to a higher strain hardening exponent and hardening capacity. Unlike the extruded magnesium alloys, the SiCp/AA2009 composite exhibited symmetrical hysteresis loops in tension and compression due to the dislocation slip-dominated deformation in the aluminum matrix. Cyclic hardening occurred at higher strain amplitudes with a more pronounced hardening in the T4 condition, and cyclic stabilization remained at lower strain amplitudes (0.1–0.3%). Fatigue life in both conditions was equivalent, which can be well described by the Coffin–Manson law and Basquin's equation. Strain ratio significantly affected cyclic deformation characteristics of the composites in both conditions, with a large amount of plastic deformation observed in the tensile phase of the first cycle of hysteresis loops at zero or positive strain ratios. A mean stress relaxation was observed. Fatigue crack was observed to initiate from the specimen surface and crack propagation was characterized predominantly by particle cracking along with debonding.

1. Introduction

Due to the tremendous environmental concerns and rising global energy demand in recent years, lightweighting of vehicles is being deemed as a prime design tool for improving the fuel economy and reducing anthropogenic environment-damaging, climate-changing, costly and human death-causing[1] emissions [1–5]. It has also been reported that the fuel efficiency of passenger vehicles can be improved by 6–8% for each 10% reduction in weight [6–9]. This has drawn a considerable interest in the application of lightweight metals and alloys in the automotive and aerospace industry [10]. Metal-matrix composites (MMCs) are one of the attractive lightweight materials since they can offer significant weight reduction and improve fuel efficiency due to their excellent combination of physical and mechanical properties, such as low density, high tensile strength, enhanced stiffness, superior wear and creep properties, as well as improved fatigue resistance compared with their counterpart monolithic alloys [11–17]. MMCs, such as aluminum matrix composites (AMCs) reinforced with ceramic particles, often silicon carbide (SiCp), have found a lot of applications in the automotive industry for the production of pistons, cylinder liners, cam shafts, connecting rods, main bearings, brake rotors and calipers, and in the aerospace industry for the production of structural components [18]. AMCs can be reinforced with continuous fiber or discontinuous particles or whiskers. Compared with the long fiber reinforced AMCs, particle-reinforced AMCs are rapidly developed because of their lower costs, isotropic properties, and desirable deformability [19,20]. The structural application of the AMCs involves inevitably fatigue and cyclic deformation characteristics due to the fact that structural components experience dynamic loading, which results in the occurrence of fatigue failure [14,15,21–26]. Hence, an understanding of fatigue and cyclic deformation behavior of AMCs is critical for the design, durability evaluation and life prediction of engineering components.

Studies have been conducted to understand the influence of particulate reinforcements on high cycle fatigue (HCF) behavior [27,28] and tensile fracture behavior [12,29] of AMCs. Several studies also

* Corresponding authors. Tel.: +1 (416) 979 5000x6487; fax: +1 (416) 979 5265 (D.L. Chen). Tel./fax: +86 24 83978908 (Z.Y. Ma).
E-mail addresses: dchen@ryerson.ca (D.L. Chen), zyma@imr.ac.cn (Z.Y. Ma).

[1] According to Science News entitled "Air pollution kills 7 million people a year" on March 25, 2014 at http://news.sciencemag.org/signal-noise/2014/03/air-pollution-kills-7-million-people-year: "Air pollution is not just harming Earth; it is hurting us, too. Startling new numbers released by the World Health Organization today reveal that one in eight deaths are a result of exposure to air pollution. The data reveal a strong link between the tiny particles that we breathe into our lungs and the illnesses they can lead to, including stroke, heart attack, lung cancer, and chronic obstructive pulmonary disease."

http://dx.doi.org/10.1016/j.matdes.2014.10.070
0261-3069/

reported the effect of particulate reinforcements on LCF behavior of AMCs [11,13–15,30,31], e.g., cyclic plastic strain response and fracture behavior of AMCs reinforced with Al_2O_3p [15,31] and SiCp [11,13,14,30], respectively. Uyger and Külekcì [14] reported the influence of volume fraction, particulate size and strain ratio on the LCF behavior of SiCp/AA2124-T4 composites. Srivatsan et al. [11] also reported the effects of temperature on the LCF properties and fracture characteristics of an AMCs reinforced composite with SiCp. In addition, high cycle fatigue resistance and tensile properties of friction stir welded SiCp/AA2009 composites were also reported by Ni et al. [32,33]. To the authors' knowledge, no systematic studies have been conducted to understand the effect of heat treatment conditions on the LCF behavior of AMCs reinforced with SiCp. It is unclear whether these composites exhibit cyclic hardening or softening and how the heat treatment and strain ratio affect the tensile-compressive yield symmetry and fatigue life. The present study was, therefore, aimed at exploring the cyclic deformation behavior of an extruded Al–Cu–Mg aluminum alloy reinforced with SiCp (SiCp/AA2009) in T4 and T6 temper at varying strain amplitudes and strain ratios.

2. Material and experimental procedure

The material used in the present investigation was an aluminum alloy (designated by the Aluminum Association as AA2009) based composite reinforced with 17 vol.% SiCp. The chemical composition of the AA2009 alloy was: 4.0 Cu-1.5 Mg (wt.%). SiCp with an average particle size of ~7 μm were adopted. The composite material was produced by powder metallurgy and the hot pressed ingot was extruded into plates of 30 mm × 200 mm. The extruded material was then subjected to (a) T4 heat-treatment: solutionized at 515 °C for 1 h, water quenched, and then aged at room temperature, and (b) T6 heat-treatment: solutionized at 515 °C for 1 h, water quenched, and then aged at 175 °C for 6 h, respectively.

Microstructural examinations were performed using an optical microscope (OM) equipped with Clemex quantitative image analysis software and a scanning electron microscope (SEM) JSM-6380LV equipped with an Oxford energy dispersive X-ray spectroscopy (EDS) system. Standard metallographic sample preparation techniques were used with an etchant based on Keller's reagent containing 10 ml hydrofluoric acid, 30 ml nitric acid, and 50 ml H_2O. X-ray diffraction tests for phase identification were conducted with Cu K_α radiation source at an accelerating voltage of 45 kV and a current of 40 mA.

Sub-sized fatigue samples, which had a gauge length of 25 mm (or a parallel length of 32 mm) and a cross section of 6 mm × 6 mm in the gauge area, were machined with the length of the samples parallel to the extrusion direction (ED). The gage section of fatigue samples was ground along the loading direction with emery papers up to a grit number of 600 to remove the machining marks and to achieve a consistent surface.

Strain-controlled, pull–push type fatigue tests were conducted using a computerized Instron 8801 fatigue testing system via the Fast Track Low Cycle Fatigue (LCF) program at a constant strain rate of $1 \times 10^{-2}\ s^{-1}$, zero mean strain ($R_\varepsilon = -1$) and room temperature of 25 °C. Triangular loading waveform was applied during all tests. The low-cycle fatigue tests were conducted at total strain amplitudes of 0.1%, 0.2%, 0.3%, 0.4%, 0.5% and 0.6%, with at least two samples tested at each level. Additionally, to study the effect of strain ratio on the LCF behavior of the composite, tests were also carried out at five different strain ratios of $R_\varepsilon = +0.5, 0, -1, -3$, and $-\infty$. All the strain ratio tests were performed using a total strain amplitude of 0.5% and at a constant strain rate of $1 \times 10^{-2}\ s^{-1}$. The fracture surfaces of fatigued specimens were examined via SEM to identify fatigue crack initiation sites and propagation characteristics.

3. Results and discussion

3.1. Microstructure and tensile properties

Fig. 1 shows the microstructures of the extruded SiCp/AA2009 composites in different heat treatment conditions in the longitudinal (L), transverse (T), and short transverse (ST) directions. It is seen that uniform-sized SiCp were dispersed almost evenly in the AA2009 matrix. At regular intervals, some clustering and agglomeration of the reinforcing SiCp could be observed along the longitudinal orientation of the composites. It is seen that those agglomerated sites consisted of a few larger SiCp intermingled with smaller, more uniform, and regular shaped SiCp. Similar types of microstructures were also reported in extruded SiCp/AA2009/15p composites by Srivatsan et al. [11,12], 2xxx series aluminum alloy (Alcoa MB85) reinforced with 15 vol.% SiCp by Bonnen et al. [27], extruded SiC/AA2009/15p-T42 composites by Manigandana et al. [29], and extruded SiC/X2080/20p composites by Srivatsan and Prakash [13]. Though the matrix of the composites revealed grains following deep etching of the polished surfaces, the size and shape of the grains was not easily discernible at low magnifications.

X-ray diffraction patterns obtained from the T4 and T6 heat-treated samples are shown in Fig. 2. In addition to Al and SiCp peaks in both samples, Al_2CuMg peaks were also detected in the T6 heat-treated sample. This indicates that precipitates were formed when heat-treatment extended to aging treatment at 175 °C for 6 h. The presence of Al_2CuMg has been also reported in similar AMCs [34,35]. Other common precipitates, including Al_2Cu and Mg_2Si, reported in the extruded SiCp/AA2009 composites [36,37] were

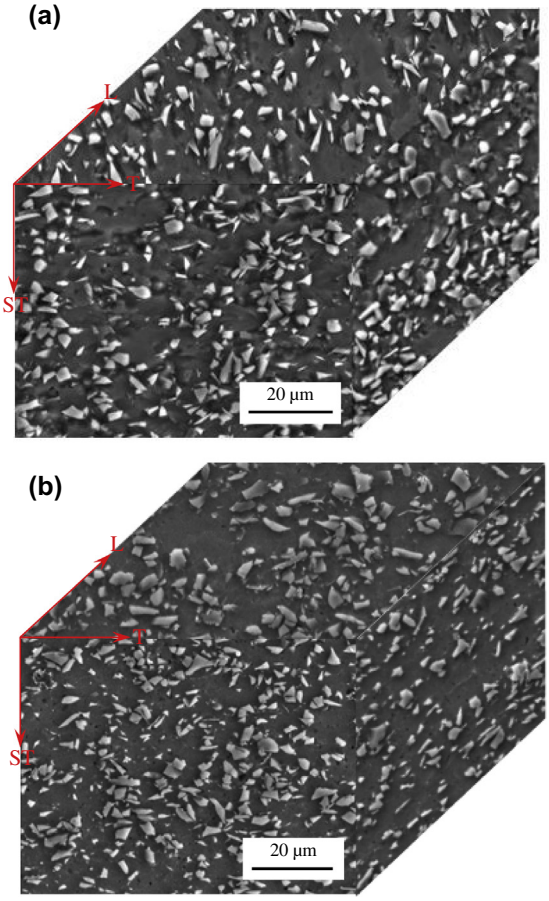

Fig. 1. Microstructures of the extruded SiCp/AA2009 composites in the longitudinal (L), transverse (T), and short transverse (ST) directions in the (a) T4, and (b) T6 conditions.

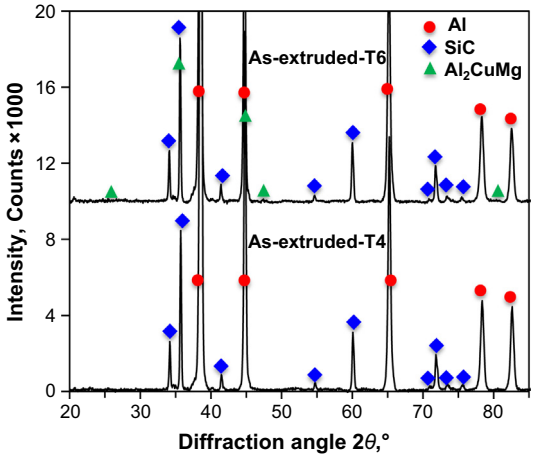

Fig. 2. X-ray diffraction patterns of heat-treated SiCp/AA2009 composites.

not seen in the XRD patterns of the present composites. Similar findings have been reported for T6 heat-treated SiCp/AA2009 composites by Rodrigo et al. [38], where it was noted that the lack of these precipitates was indicative of a good solution treatment of the composite materials.

Fig. 3 shows the typical tensile stress–strain curves of the composites determined at a strain rate of 1×10^{-3} s^{-1}. The corresponding tensile properties, i.e., the mean values based on duplicate tests, are listed in Table 1. Despite only a slight increase in the ultimate tensile strength (UTS), the T6 samples exhibited a significantly higher yield strength (YS) than the T4 samples, i.e., ~421 MPa vs. ~358 MPa, due to the presence of Al_2CuMg precipitates caused by age hardening. The slight increase in the UTS of the T6 sample was due to the fact that it did not reach its full capacity prior to failure with a ductility of 3%, in comparison with 4.4% in the T4 condition (Table 1). The obtained tensile properties were basically in agreement with those reported for extruded SiCp/AA2009 composites [11,12,29]. Young's modulus for current composites was obtained to be about 121 GPa. Using the rule of mixtures [39], the Young's modulus of the present composites could be estimated to be about 118 GPa, where the following values were used: E_m = 70 GPa (aluminum matrix) [39], E_p = 350 GPa (SiCp) [39], V_m = 0.83, and V_p = 0.17 (17 vol.% SiCp in the current composites). The estimated and measured values of Young's modulus in the current composites were in fairly good agreement. These

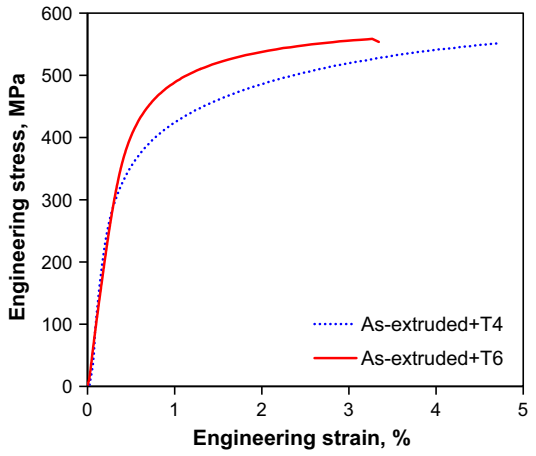

Fig. 3. Tensile stress–strain curves of the extruded SiCp/AA2009 composites in different heat-treatment conditions tested at a strain rate of 1×10^{-3} s^{-1}.

values also approximately concurred with the reported results, e.g., about 100 GPa for SiCp/AA2009 composites (15 vol.% SiCp) in the T42 condition [11,12]. The strain hardening exponent (n) evaluated according to the Hollomon equation [40] and hardening capacity (H_c) according to the equation proposed by Afrin et al. [41] are listed in Table 1. It is seen that both strain hardening exponent and hardening capacity became lower in the T6 state. This was due to the fact that the initially hardened material had a lower dislocation storage capacity. In the present T6 samples, this was mainly due to the precipitation of Al_2CuMg particles (Fig. 2). However, the strain hardening exponents obtained for the present composites in both T4 (n = 0.21) and T6 (n = 0.16) conditions were higher than that (n = 0.124) of the T42 heat-treated AA2009 alloy reinforced with 15 vol.% SiCp reported by Srivatsan et al. [12]. Similarly, the present heat-treated composites also showed significantly higher n values, as compared with the X2080 matrix alloy reinforced with 16 μm SiCp particles [13].

3.2. Cyclic deformation response

Fig. 4 shows typical stress–strain hysteresis loops of the first and mid-life cycles at a given strain amplitude of 0.6% and strain ratio of $R_\varepsilon = -1$ for the composites in different heat-treated conditions. It is seen from Fig. 4 that both the composites exhibited nearly symmetrical hysteresis loops at both the outset and mid-life, representing an isotropic response. This was in sharp contrast with the cyclic deformation characteristics in the rare-earth free extruded magnesium alloys due to the occurrence of twinning in the compressive phase caused by the presence of strong basal textures [21–23]. Such symmetrical tension–compression behavior was a result of dislocation slip-dominated deformation since the matrix material (aluminum) has face-centered cubic (fcc) crystal structure, rather than twinning often occurring in the hexagonal close-packed (hcp) metals during deformation. Similar symmetrical behavior was reported in other fcc metals (e.g., Cu, Ni) [28], SiCp/2124 [14], and Al_2O_3p/6061 [15].

Fig. 5 shows the evolution of stress amplitudes with respect to the number of cycles over a range of total strain amplitudes on a semi-log scale for the composites in different heat-treated conditions. As the total strain amplitude increased, the stress amplitude increased and the fatigue life of the material decreased in both the T4 and T6 heat-treated composites. For the T4 heat-treated composites (Fig. 5(a)), a pronounced cyclic hardening effect was observed at strain amplitudes of 0.4% and higher, whereas the composites remained cyclically stable at lower strain amplitudes (0.1–0.3%). However, for the T6 heat-treated composites (Fig. 5(b)), while the cyclic hardening tendency was remained the same, it was weaker. The variation of cyclic stress amplitude with fatigue cycling is mainly dependent on the composite microstructure and the cyclic strain amplitude applied [13]. The cyclic hardening behavior during fully reversed cyclic straining at higher strain amplitudes (Fig. 5) could be attributed to competing and synergistic effects of stress (load) transfer between the soft and ductile AA2009 matrix and the hard and brittle ceramic particle (SiCp) reinforcement [42,43], the presence of a pre-existing dislocation density in the alloy matrix caused by the presence of the SiCp [44–46], Al_2CuMg precipitates in the matrix (Fig. 2) and initial precipitate-dislocation interactions, the thermo-residual stress distribution in the composite and the related plastic strains introduced near the reinforcement particles due to mismatch in the coefficients of thermal expansion (CTE) between the soft matrix and hard SiCp particle reinforcement [47,48].

In the low cycle fatigue tests, plastic strain amplitude was considered as a physical quantity that resulted in several damaging processes and influenced the internal microstructure, which was closely related to the strain resistance and eventually the fatigue

Table 1
Tensile properties of the extruded SiCp/AA2009 composites in the T4 and T6 conditions.

Specimen	Yield strength (σ_y), MPa	Ultimate tensile strength (σ_{UTS}), MPa	Elongation, %	Strain hardening exponent (n)	Hardening capacity (H_c)[a]
As-extruded + T4	358	556	4.4	0.21	0.55
As-extruded + T6	421	559	3.0	0.16	0.33

[a] According to Afrin et al. [41] the hardening capacity H_c was defined as $H_c = \frac{\sigma_{UTS}-\sigma_y}{\sigma_y} = \frac{\sigma_{UTS}}{\sigma_y} - 1$.

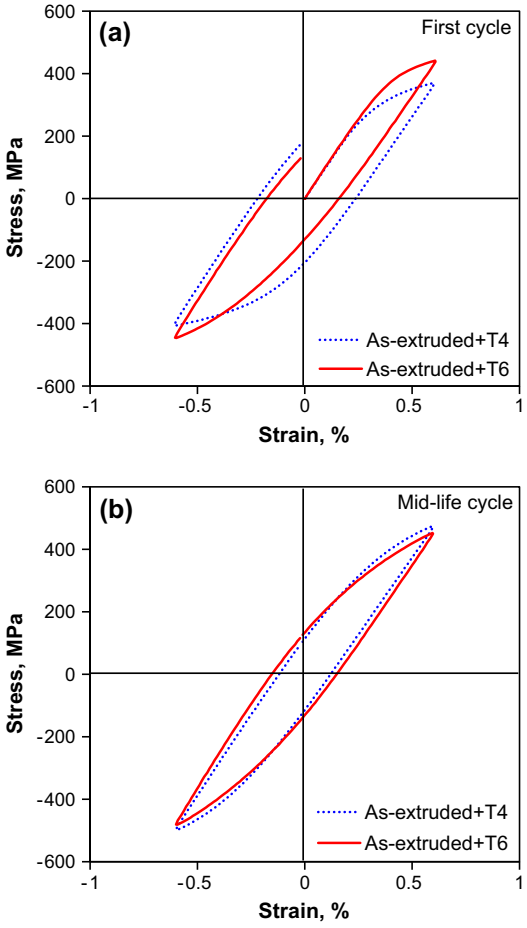

Fig. 4. Typical stress–strain hysteresis loops of the extruded SiCp/AA2009 composites at a given total strain amplitude of 0.6% and strain ratio of $R_\varepsilon = -1$, (a) first cycle, and (b) mid-life cycle.

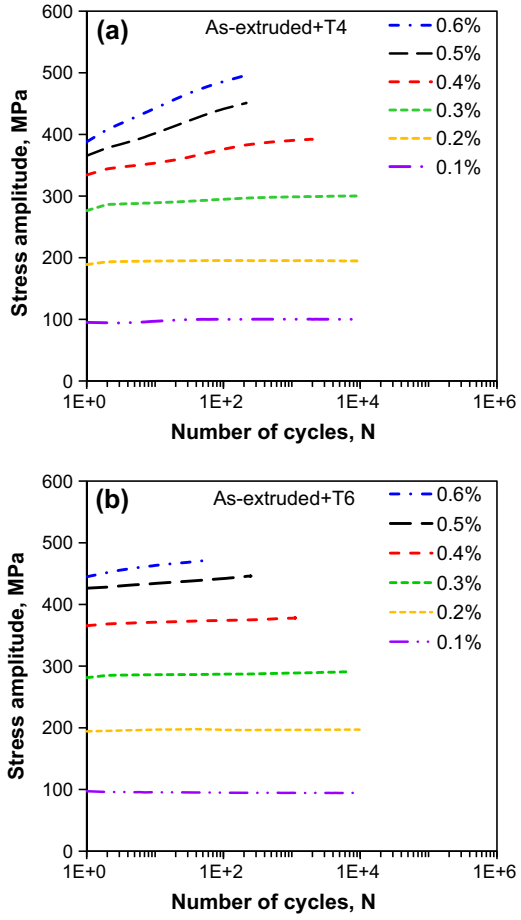

Fig. 5. Stress amplitude vs. the number of cycles for different strain amplitudes tested at a strain ratio of $R_\varepsilon = -1$ in the SiCp/AA2009 composites in the (a) T4, and (b) T6 conditions.

life [21,45,47]. The variation of the plastic strain amplitude ($\Delta\varepsilon_p/2$) during cyclic deformation is shown in Fig. 6 at different strain amplitudes for the composites in different heat-treated conditions. A decrease in the plastic strain amplitude at higher strain amplitudes (Fig. 6) corresponded well to an increase in the stress amplitude (Fig. 5) in both composites. As with the stress amplitude, the plastic strain amplitude remained cyclically stable at lower strain amplitudes. The cyclic hardening at higher strain amplitudes, as indicated by the decrease in the plastic strain amplitude, was stronger in the T4 state than in the T6 state. This was closely related to the higher monotonic strain hardening exponent and hardening capacity (H_c) in the T4 condition (Table 1). Furthermore, while the initial cyclic deformation characteristics were similar (i.e., cyclic hardening occurred) in both heat-treated conditions, both the cyclic stress amplitudes and plastic strain amplitudes at a given total strain amplitude were different, except at lower strain amplitudes of 0.1–0.3%. For example, at a total strain amplitude of 0.5% the stress amplitude was ~369 MPa in the T4 state, and ~415 MPa in the T6 state (Fig. 5). The difference in the stress amplitude also increased with increasing strain amplitude applied.

3.3. Fatigue life and fatigue parameters

The total strain amplitudes ($\Delta\varepsilon_t/2$) as a function of the fatigue life (i.e., the number of cycles to failure, N_f) is plotted in Fig. 7, in comparison with the data reported in the literature for various Al composites [13–15,30,31]. As seen from Fig. 7, the present composites in both heat-treated conditions had more or less the same fatigue lives. It is also seen that the present SiCp/AA2009 composites were stronger than several existing Al composites and comparable to even those materials reinforced with ultra-fine particles. Specifically, the fatigue life of the present composites was significantly higher at all strain amplitudes than that of a similar as-cast SiCp reinforced A356 composite [30], SiCp reinforced Al–Cu–Mg–Zr (X2080) composite [13], AA2009 composite reinforced with 20 vol.% SiCp [31], and (Al_2O_3 + TiB_2)/Al composite [31]. Similar improvements in the fatigue life was also observed for spray-atomized SiCp reinforced AA2009 composites [30] and Al–Cu–Mg–Mn (2124) composite reinforced with sub-micron scale SiCp [14]. However, aluminum alloys reinforced with ultra-fine SiCp (i.e., with an average particle size of 0.7 μm) were found to have slightly

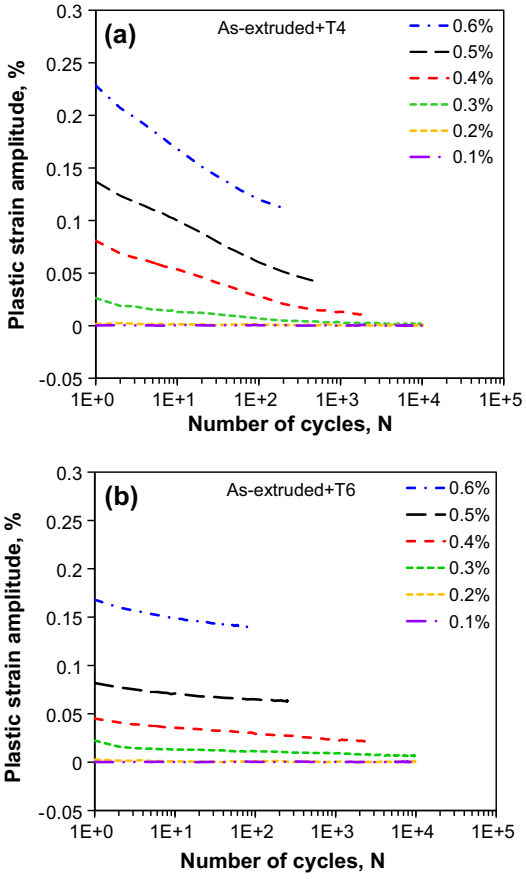

Fig. 6. Plastic strain amplitude vs. the number of cycles for different strain amplitudes tested at a strain ratio of $R_\varepsilon = -1$ in the SiCp/AA2009 composites in the (a) T4, and (b) T6 conditions.

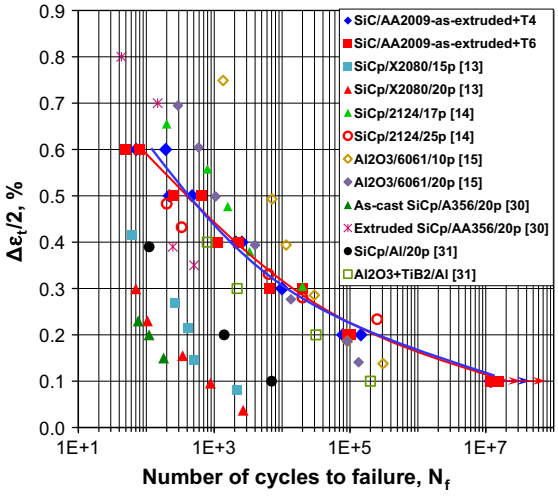

Fig. 7. Total strain amplitude versus the number of cycles to failure of the extruded SiCp/AA2009 composites, in comparison with the data reported in the literature for various Al composites.

longer fatigue life than the present SiCp/AA2009 composites [14,15]. This was due to the fact that ultra-fine particles could restrict the movement of dislocations most effectively. The improved fatigue resistance of the present SiCp/AA2009 composites indicated that the volume fraction of 17% and choice of reinforcement (i.e., 7 μm SiCp) resulted in optimal interfacial matrix-particle bonding.

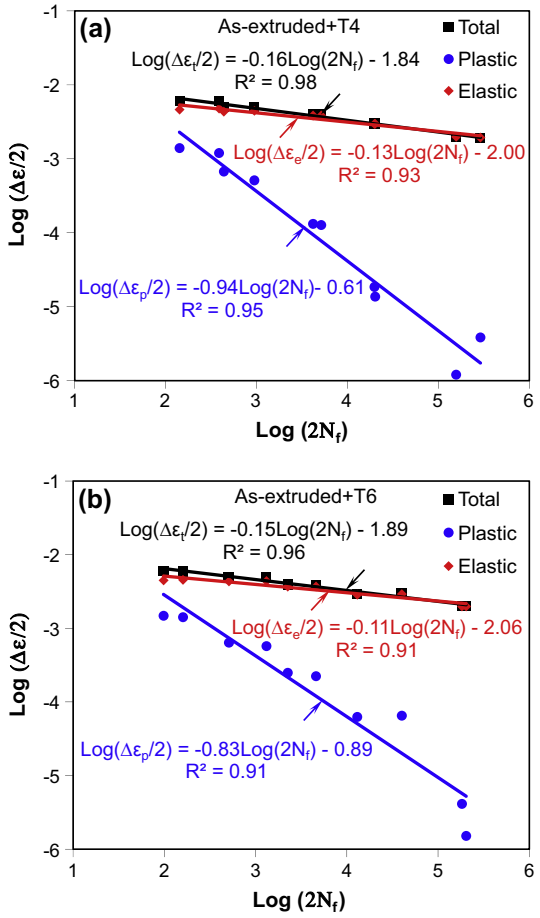

Fig. 8. Cyclic total, plastic, and elastic strain amplitude-fatigue life response of the SiCp/AA2009 composites in the (a) T4, and (b) T6 conditions.

Based on the Basquin equation and Coffin–Manson relation, the total strain amplitude could be expressed as two components of elastic strain amplitude and plastic strain amplitude [23–25,49–51], i.e.,

$$\frac{\Delta\varepsilon_t}{2} = \frac{\Delta\varepsilon_e}{2} + \frac{\Delta\varepsilon_p}{2} = \frac{\sigma_f'(2N_f)^b}{E} + \varepsilon_f'(2N_f)^c, \quad (1)$$

where E is the Young's modulus, N_f is the fatigue life or number of cycles to failure, σ_f' is the fatigue strength coefficient, b is the fatigue strength exponent, ε_f' is the fatigue ductility coefficient, and c is the fatigue ductility exponent. In addition, cyclic deformation behavior is normally considered to be predominantly dependent on the portion of the plastic strain amplitude and independent of the elastic strain amplitude, which could be expressed by the following equation [23],

$$\frac{\Delta\sigma}{2} = K'\left(\frac{\Delta\varepsilon_p}{2}\right)^{n'}, \quad (2)$$

where $\frac{\Delta\sigma}{2}$ is the mid-life stress amplitude, $\frac{\Delta\varepsilon_p}{2}$ is the mid-life plastic strain amplitude, n' is the cyclic strain-hardening exponent and K' is the cyclic strength coefficient. Fig. 8 presents the total, elastic and plastic strain amplitudes as a function of the number of reversals to failure ($2N_f$) for the extruded SiCp reinforced AA2009 matrix composites in different heat-treated conditions, where the values of the strain amplitudes were taken from the mid-life cycles. The fatigue life parameters in both extruded composites evaluated on the basis of Eqs. (1) and (2) are summarized in Table 2. It is seen from Fig. 8 that the Basquin and Coffin–Manson relations are obeyed fairly well, and the obtained fatigue parameters were in agreement

Table 2
Low cycle fatigue parameters obtained for the extruded SiCp/AA2009 composites in the T4 and T6 conditions.

Low cycle fatigue parameter	As-extruded + T4	As-extruded + T6
Cyclic strain hardening exponent, n'	0.13	0.14
Cyclic strength coefficient, K', MPa	1139	1181
Fatigue strength coefficient, σ'_f, MPa	1010	899
Fatigue strength exponent, b	−0.13	−0.11
Fatigue ductility coefficient, ε'_f	0.25	0.13
Fatigue ductility exponent, c	−0.95	−0.83

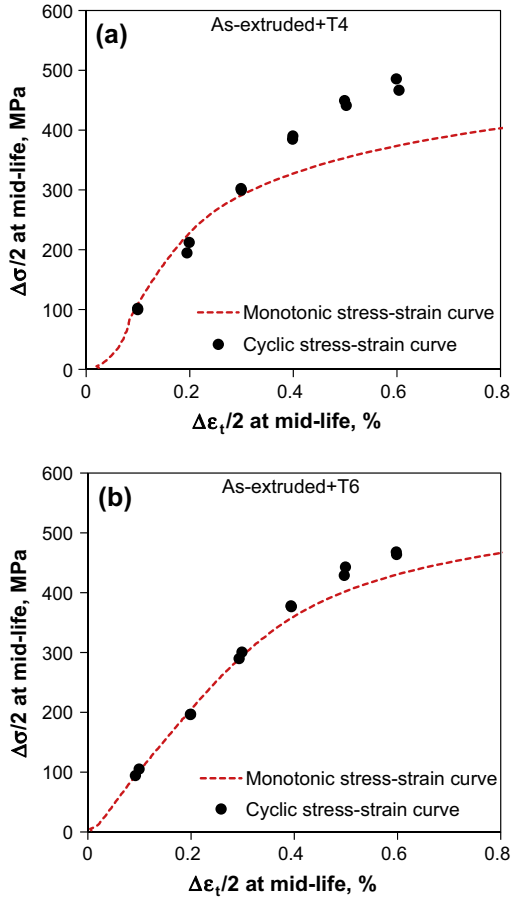

Fig. 9. Cyclic stress–strain curves for SiCp/AA2009 composites in the (a) T4, and (b) T6 conditions, where the corresponding monotonic stress–strain curves are plotted for comparison.

with the data of other Al composites reported in the literature [11,13,15], except for the cyclic strength coefficient (K') which was higher than the reported data. Fig. 9 shows the monotonic and cyclic stress–strain curves of the T4 and T6 heat-treated samples. The steeper slope of the cyclic stress–strain curves in both conditions demonstrated a more pronounced hardening effect in the extruded AA2009 composite in the cyclic loading than the monotonic tensile loading, especially in the T4 condition. This hardening behavior could be attributed to the interactions of dislocations during deformation in the plastic domain [11]. More specifically, dislocation multiplication during deformation increased the dislocation density in the matrix and subsequently increased the interactions among dislocations, as well as interactions between dislocations and the SiCp particles [11]. The situation shown in Fig. 9 where the cyclic stress–strain curve is positioned above the monotonic stress–strain curve indeed reflects cyclic hardening behavior of a material, as noted in [49]. This corresponded well to the change

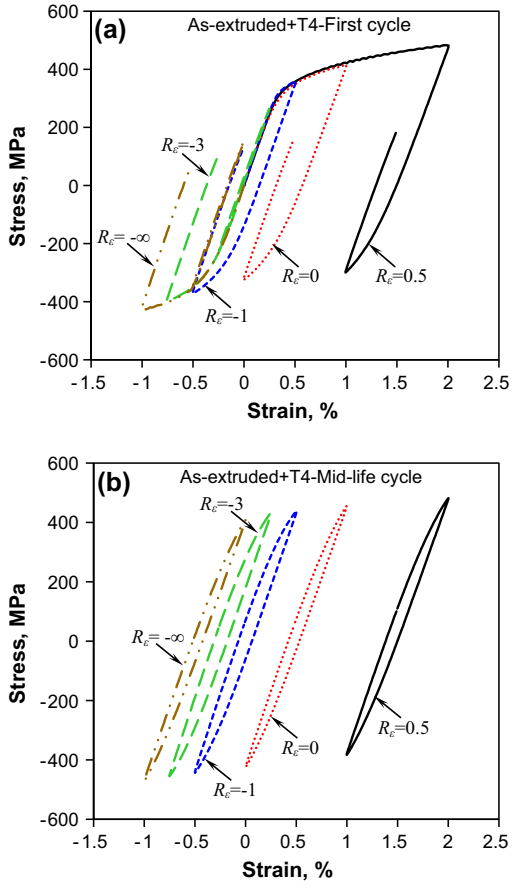

Fig. 10. Typical stress–strain hysteresis loops of different cycles for different strain ratios at a given total strain amplitude of 0.5% of SiCp/AA2009 composites in the T4 state, (a) first cycle, and (b) mid-life cycle.

in the cyclic stress amplitude and plastic strain amplitude (Figs. 5 and 6). It is also well known that materials with a high monotonic strain hardening exponent ($n > 0.15$) undergo cyclic hardening; those with a low monotonic strain hardening exponent ($n < 0.15$) experience cyclic softening. As seen from Table 1, the present composites had a monotonic strain hardening exponent of 0.21 in the T4 condition and 0.16 in the T6 condition. It follows that cyclic hardening occurred in both conditions, with T4 condition exhibiting a higher extent of cyclic hardening than T6 condition, as seen from Figs. 5, 6 and 9.

3.4. Effect of strain ratio on LCF

Figs. 10 and 11 show typical stress–strain hysteresis loops of the (a) first and (b) mid-life cycles at different strain ratios, R_ε, and at a given strain amplitude of 0.5% in the T4 and T6 heat-treated SiCp/AA2009 composites, respectively. It is seen from Figs. 10 and 11(a) that at all strain ratios in both conditions, the initial tensile phase of the first cycle was synchronized and followed essentially the same path, which suggested the occurrence of Masing-like behavior, representing a special cyclic stress–strain response in some materials as reported by Chirst and Mughrabi [52]. It was also reported that Masing behavior appeared due to the lack of significant microstructural changes during the fatigue tests performed for different strain ratios [53,54]. With increasing strain ratio from $-\infty$ (negative infinity) to 0.5, the maximum/peak tensile stress σ_{max} increased from nearly zero to about 480 MPa (Fig. 10(a)) and to about 530 MPa (Fig. 11(a)) in the T4 and T6 heat-treated SiCp/AA2009 composites, respectively, and the plastic deformation in

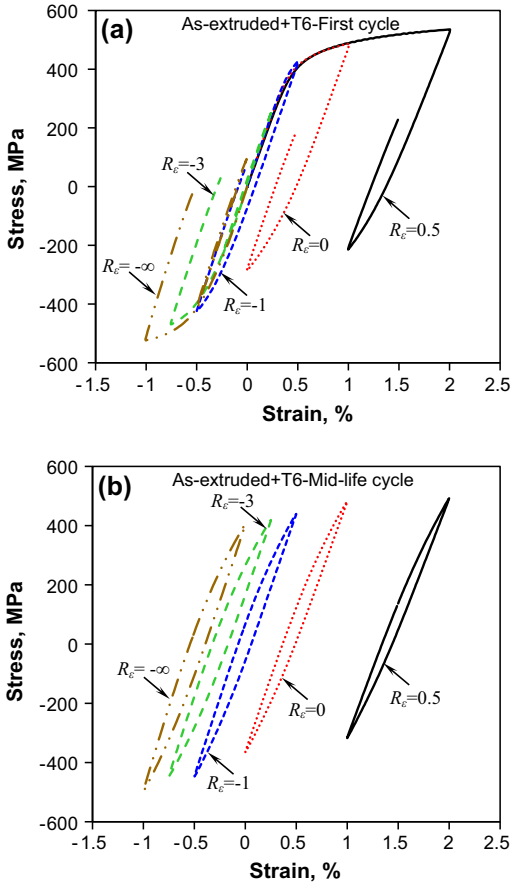

Fig. 11. Typical stress–strain hysteresis loops of different cycles for different strain ratios at a given total strain amplitude of 0.5% of SiCp/AA2009 composites in the T6 state, (a) first cycle, and (b) mid-life cycle.

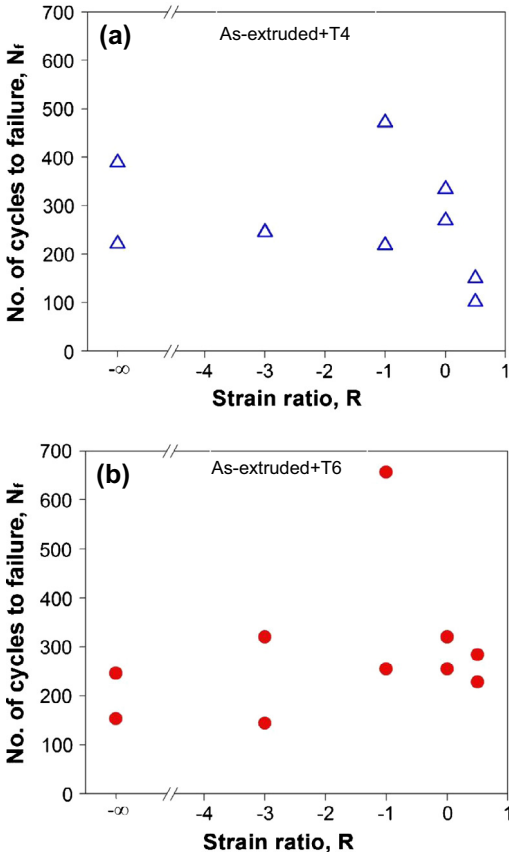

Fig. 12. Number of cycles to failure vs. strain ratio of SiCp/AA2009 composites in the (a) T4 and (b) T6 conditions at a given total strain amplitude of 0.5% and strain rate of 1×10^{-2} s^{-1}.

the tensile phase became much more remarkable in both conditions (Figs. 10 and 11(a)). To be more specific, a large amount of plastic deformation appeared in the tensile phase for zero or positive strain ratio (i.e., $R_\varepsilon = 0$ and 0.5). This was attributed to the high positive mean strain values, which forced the occurrence of a large amount of plastic deformation in the tensile and compressive phase of the first cycles. The significantly larger shifts of the hysteresis loops from $R_\varepsilon = 0$ to $R_\varepsilon = 0.5$ were also due to the influence of strain limits. As the strain ratio was reduced from 0.5 to $-\infty$, the peak compressive stress σ_{min} decreased from about −290 MPa to about −420 MPa (Fig. 10(a)) and from about −200 MPa to about −520 MPa (Fig. 11(a)) in the T4 and T6 heat-treated samples, respectively. Tests performed at $R_\varepsilon = 0.5$ and $R_\varepsilon = 0$ did not reach the compressive yielding point of the present composites due to the high positive lower strain limits (i.e., $\varepsilon_{min} = 1\%$ for $R_\varepsilon = 0.5$ and $\varepsilon_{min} = 0$ for $R_\varepsilon = 0$). It is seen from Figs. 10 and 11(b) that the mid-life cycles shifted towards the zero-stress line due to the occurrence of mean stress relaxation to a certain extent. While the $R_\varepsilon = -1$ test gave essentially symmetrical hysteresis loops, the tests at other strain ratios apparently gave rise to slight asymmetrical hysteresis loops with respect to the zero-stress line (Figs. 10 and 11(b)). However, these results differed from those in the extruded magnesium alloys, in which twinning–detwinning activities resulted in asymmetric hysteresis loops reported in [21–23].

Fig. 12 shows the fatigue life (i.e., the number of cycles to failure, N_f) as a function of strain ratio in the T4 and T6 heat-treated samples. It is seen that in both cases, the fatigue life appeared to be highest at $R_\varepsilon = -1$, while it decreased as the strain ratio deviated both positively and negatively from $R_\varepsilon = -1$. This suggests that the strength of the material is optimized when uniform tensile and compressive stresses are applied (i.e., with a mean stress of zero at $R_\varepsilon = -1$). The mean stress of the T4 and T6 heat-treated samples as a function of normalized cycle ratio (N/N_f), where N_f is the fatigue life (the number of cycles to failure), is shown in Fig. 13. As the normalized cycle ratio N/N_f increased, the mean stress decreased for $R_\varepsilon > -1$ and increased for $R_\varepsilon < -1$. That is, the mean stress tended to become closer to zero. Quasi-stabilization of these curves occurred after ~10–20% of the fatigue life. Accordingly, the strength of the material may be related to how effectively the sample was able to approach a zero mean stress. This phenomenon is often referred to as the mean stress relaxation. It is clear that the mean stress relaxation occurred more drastically at the outset of cyclic deformation within the initial cycles of the fatigue life, beyond which (especially beyond the mid-life) it became increasingly stabilized. The mean stress at $R_\varepsilon = -1$ remained fairly stable at nearly zero. The absolute value of the maximum mean stress was ~100 MPa and ~200 MPa for the T4 and T6 heat-treated samples, respectively. This was associated with the higher strength of the composites in the T6 condition. Similar findings have been reported for 2124 Al-alloy T4 composites reinforced with SiCp particles [14].

3.5. Fractography

Fig. 14 shows an overall view of the fracture surfaces at a lower magnification in the T4 and T6 conditions tested at a total strain amplitude of 0.2%. The propagation area can be classified into three major regions based on the slightly different colors; (i) the area near the crack initiation site, (ii) the intermediate propagation area, and (iii) the final fast fracture region. Fatigue crack initiation

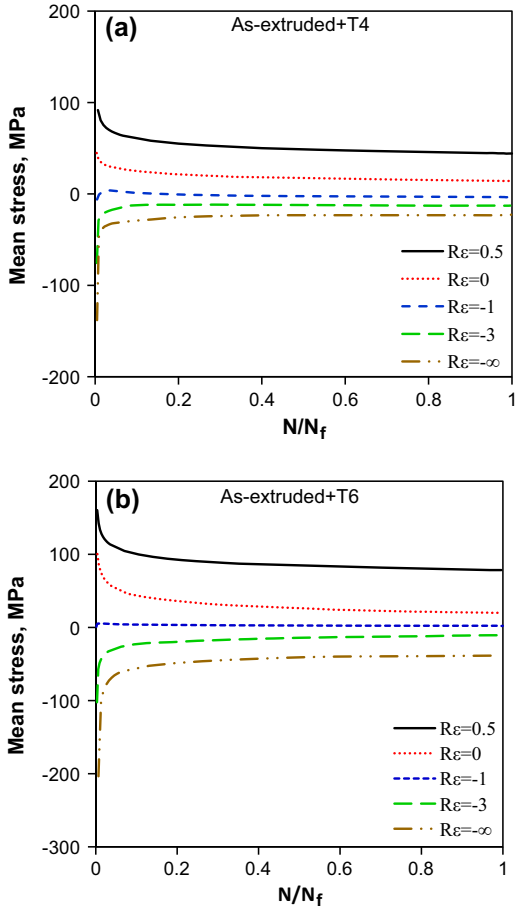

Fig. 13. Mean stress vs. a normalized cycle ratio (N/N_f) of SiCp/AA2009 composites in the (a) T4 and (b) T6 conditions at different strain ratios at a total strain amplitudes of 0.5%.

was observed to occur from the specimen surface. This could be better seen from Fig. 15, where the crack growth near the initiation site appeared to occur primarily through the matrix, with no evidence of particle/matrix interfacial cracking or particle cracking. Figs. 16 and 17 show the intermediate propagation region tested at a total strain amplitude of 0.2% for the T4 and T6 heat-treated specimens, respectively, at a higher magnification. The composites in both T4 and T6 conditions exhibited a similar fractograph. The location and orientation of fractured SiCp particles could be clearly identified from the SEM back-scattered electron images (Figs. 16 and 17(b)), while the topography of the fracture surface could be observed from the SEM secondary electron images (Figs. 16 and 17(a)). SiCp cracking, indicated by the arrows in Figs. 16 and 17, was the predominant failure mechanism observed, indicating a strong interfacial bonding between SiCp and the AA2009 matrix, in spite of the occurrence of particle de-cohesion as well. Similar fracture characteristics were also reported for similar SiCp/AA2009 composites [11,12].

4. Conclusions

Strain-controlled low cycle fatigue tests were conducted on extruded SiCp/AA2009 composites in different heat treatment conditions of T4 and T6 at varying strain amplitudes and strain ratios. The following conclusions can be drawn from this investigation:

(1) Microstructural observations of the SiCp/AA2009 composites revealed even-sized SiCp uniformly dispersed throughout the AA2009 matrix, with little agglomerated sites observed. After T6 heat treatment, Al_2CuMg precipitates appeared.
(2) In comparison with the T6 condition, while the SiCp/AA2009 composite in the T4 condition exhibited a lower yield strength, it had a higher ductility and equivalent ultimate tensile strength. This gave rise to a higher strain hardening exponent and hardening capacity in the T4 condition.
(3) The SiCp/AA2009 composites exhibited basically symmetrical hysteresis loops in tension and compression, representing an isotropic response in the composites. This was due to the dislocation slip-dominated deformation in face-centered cubic (fcc) aluminum matrix, rather than twinning in the hcp metals.
(4) Cyclic hardening was observed at strain amplitudes of 0.4% and higher in both T4 and T6 conditions, with a more pronounced hardening in the T4 condition. The hardening behavior was mainly attributed to the interactions of dislocations in the plastic domain and the resistance of SiCp during cyclic deformation. Cyclic stabilization occurred at lower strain amplitudes (0.1–0.3%).
(5) The fatigue life of the SiCp/AA2009 composites in both T4 and T6 conditions was equivalent within the experimental scatter, which can be well described by the Coffin–Manson law and Basquin's equation.
(6) Strain ratio significantly affected the cyclic deformation characteristics of the composites in both T4 and T6 conditions. A large amount of plastic deformation occurred in

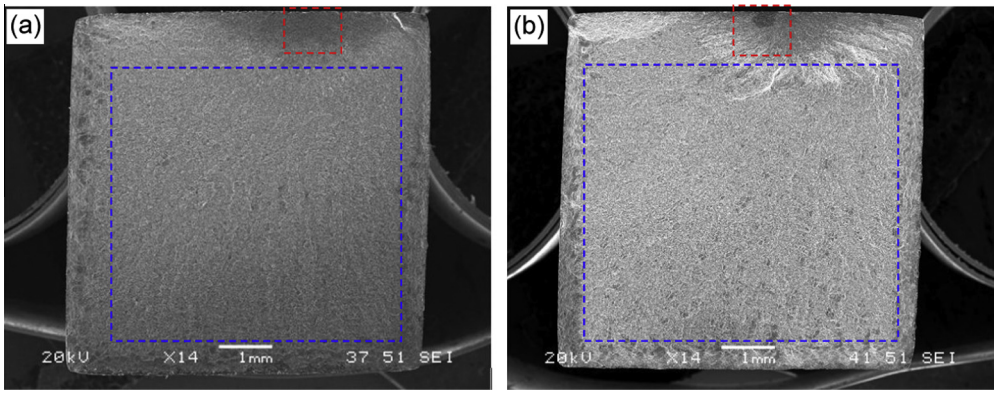

Fig. 14. SEM images of overall fracture surfaces of SiCp/AA2009 composites in the (a) T4 and (b) T6 conditions fatigued at a total strain amplitude of 0.2%.

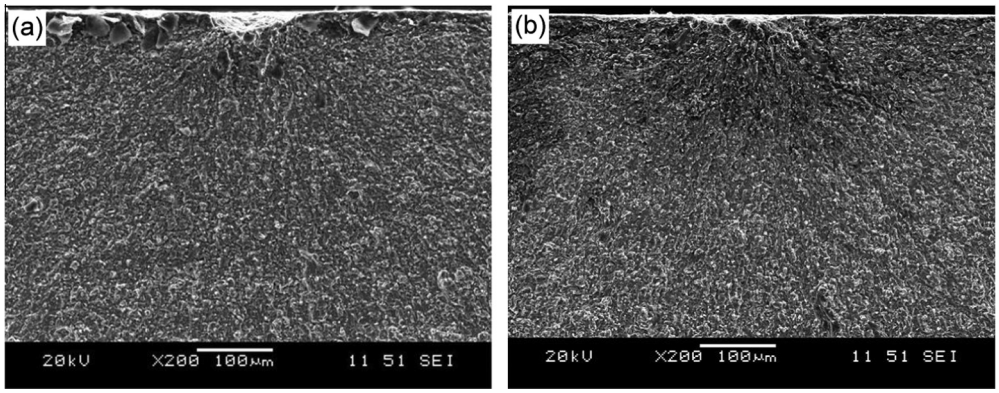

Fig. 15. SEM micrographs of the fracture surfaces near fatigue crack initiation site of SiCp/AA2009 composites in the (a) T4 and (b) T6 conditions fatigued at a total strain amplitude of 0.2%.

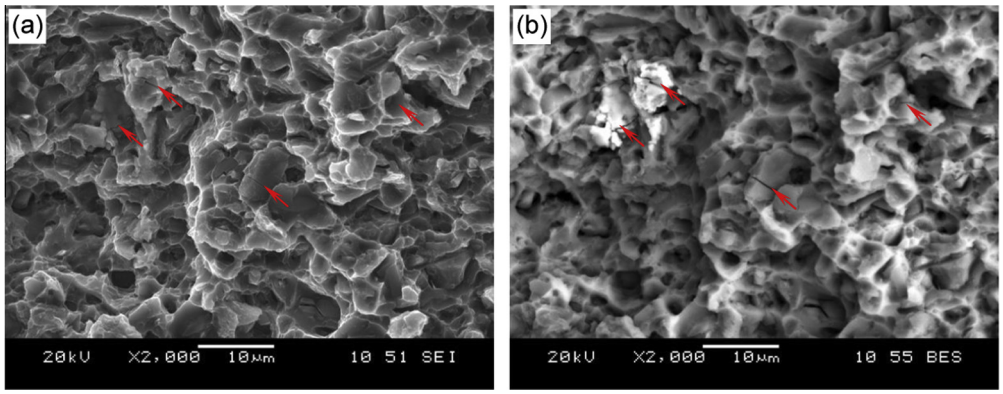

Fig. 16. (a) SEM secondary electron and (b) back-scattered electron micrographs of the fatigue crack propagation region of the T4 heat-treated specimen fatigued at a total strain amplitude of 0.2%.

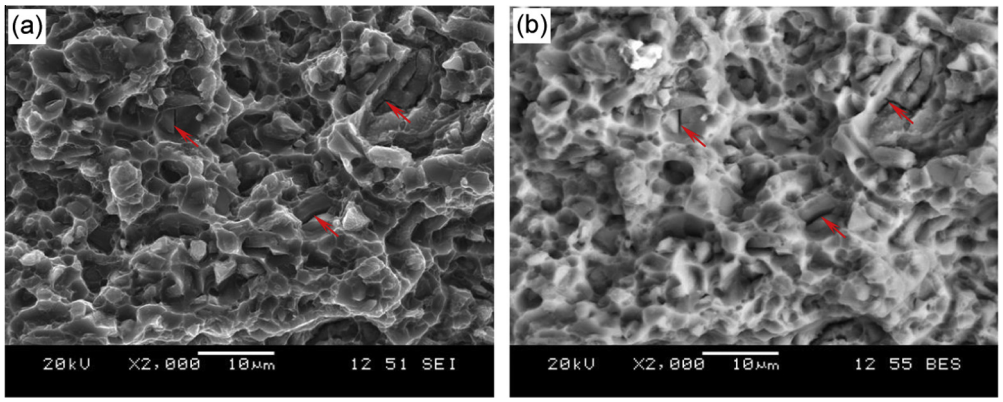

Fig. 17. (a) SEM secondary electron and (b) back-scattered electron micrographs of the fatigue crack propagation region of the T6 heat-treated specimen fatigued at a total strain amplitude of 0.2%.

the tensile phase of the first cycle of hysteresis loops at zero or positive strain ratio (i.e., $R_\varepsilon = 0$ and 0.5), which was related to the high positive mean strain values.

(7) Fatigue crack initiation was observed to occur from the specimen surface. SiCp particle cracking was the predominant failure mechanism observed, indicating a strong interfacial bonding between SiCp and the AA2009 matrix. Additionally, some particle de-cohesion was also observed in the intermediate propagation area.

Acknowledgements

The authors would like to thank the Natural Sciences and Engineering Research Council of Canada (NSERC) for providing financial support. Z.Y. Ma would like to give thanks to National Basic Research Program of China for the financial support (Grant No. 2012CB619600). D.L. Chen is also grateful for the financial support by the Premier's Research Excellence Award (PREA), NSERC-Discovery Accelerator Supplement (DAS) Award, Canada

Foundation for Innovation (CFI), and Ryerson Research Chair (RRC) program. The authors would also like to thank Messrs. A. Machin, Q. Li, J. Amankrah and R. Churaman for easy access to the laboratory facilities of Ryerson University and their assistance in the experiments.

References

[1] McNutt M. Climate change impacts. Science 2013;341:435.
[2] Pollock TM. Weight loss with magnesium alloys. Science 2010;328:986–7.
[3] Revesz RL, Howard PH, Arrow K, Goulder LH, Kopp RE, Livermore MA, et al. Global warming: improve economic models of climate change. Nature 2014;508:173–5.
[4] Murray J, King D. Oil's tipping point has passed. Nature 2012;481(7382):433–5.
[5] Myers SS, Zanobetti A, Kloog I, Huybers P, Leakey ADB, Bloom AJ, et al. Increasing CO_2 threatens human nutrition. Nature 2014;510:139–42.
[6] Mirza FA, Chen DL, Li DJ, Zeng XQ. Effect of strain ratio on cyclic deformation behavior of a rare-earth containing extruded magnesium alloy. Mater Sci Eng A 2013;588:250–9.
[7] Tahreen N, Chen DL, Nouri M, Li DY. Effects of aluminum content and strain rate on strain hardening behavior of cast magnesium alloys during compression. Mater Sci Eng A 2014;594:235–45.
[8] Macwan A, Patel VK, Jiang XQ, Li C, Bhole SD, Chen DL. Ultrasonic spot welding of Al/Mg/Al tri-layered clad sheets. Mater Des 2014;62:344–51.
[9] Sarker D, Friedman J, Chen DL. Influence of pre-deformation and subsequent annealing on strain hardening and anisotropy of AM30 magnesium alloy. J Alloys Compd 2014;611:341–50.
[10] Patel HA, Chen DL, Bhole SD, Sadayappan K. Low cycle fatigue behavior of a semi-solid processed AM60B magnesium alloy. Mater Des 2013;49:456–64.
[11] Srivatsan TS, Al-Hajri M, Vasudevan VK. Cyclic plastic strain response and fracture behavior of 2009 aluminum alloy metal-matrix composite. Int J Fatigue 2005;27:357–71.
[12] Srivatsan TS, Al-Hajri M, Vasudevan VK, Smith C, Petraroli M. The tensile response and fracture behavior of 2009 aluminum alloy metal matrix composite. Mater Sci Eng A 2003;346:91–100.
[13] Srivatsan TS, Prakash A. Effect of particulate silicon carbide on cyclic strain resistance and fracture behavior of X2080 aluminum alloy metal matrix composites. Eng Fract Mech 1994;49(5):751–72.
[14] Uygur I, Külekcī MK. Low cycle fatigue properties of 2124/SiCp Al-alloy composites. Turkish J Eng Env Sci 2002;26:265–74.
[15] Gasem ZM, Ali SS. Low-cycle fatigue behavior of powder metallurgy 6061 aluminum alloy reinforced with submicron-scale Al_2O_3 particles. Mater Sci Eng A 2013;562:109–17.
[16] Akbarpour MR, Salahi E, Alikhani Hesari F, Kim HS, Simchi A. Effect of nanoparticle content on the microstructural and mechanical properties of nano-SiC dispersed bulk ultrafine-grained Cu matrix composites. Mater Des 2013;52:881–7.
[17] Asif Iqbal AKM, Arai Y, Araki W. Effect of hybrid reinforcement on crack initiation and early propagation mechanisms in cast metal matrix composites during low cycle fatigue. Mater Des 2013;45:241–52.
[18] Macke A, Schultz BF, Rohatgi PK, Gupta N. Metal matrix composites for automotive applications. In: Elmarakbi A, editor. Advanced composite materials for automotive applications: structural integrity and crashworthiness. Chichester, UK: John Wiley & Sons Ltd; 2013.
[19] Ibrahim IA, Mohamed FA, Lavernia EJ. Particulate reinforced metal matrix composites - a review. J Mater Sci 1991;26(5):1137–56.
[20] Tjong SC, Ma ZY. Microstructural and mechanical characteristics of in situ metal matrix composites. Mater Sci Eng R 2000;29:49–113.
[21] Begum S, Chen DL, Xu S, Luo AA. Low cycle fatigue properties of an extruded AZ31 magnesium alloy. Int J Fatigue 2009;31:726–35.
[22] Begum S, Chen DL, Xu S, Luo AA. Strain-controlled low-cycle fatigue properties of a newly developed extruded magnesium alloy. Metall Mater Trans A 2008;39:3014–26.
[23] Lin XZ, Chen DL. Strain controlled cyclic deformation behavior of an extruded magnesium alloy. Mater Sci Eng A 2008;496:106–13.
[24] Mirza FA, Chen DL. In: Zhang S, Zhao DL, editors. Aerospace Materials Handbook. New York: CRC Press, Taylor & Francis; 2013.
[25] Patel HA, Chen DL, Bhole SD, Sadayappan K. Cyclic deformation and twinning in a semi-solid processed AZ91D magnesium alloy. Mater Sci Eng A 2010;528:208–19.
[26] Anand D, Chen DL, Bhole SD, Andreychuk P, Boudreau G. Fatigue behavior of tailor (laser) welded blanks for automotive applications. Mater Sci Eng A 2006;420(1–2):199–207.
[27] Bonnen JJ, Allison JE, Jones JW. Fatigue Behavior of a 2xxx Series Aluminum Alloy Reinforced with 15 Vol Pct SiCp. Metall Trans A 1991;22A:1007–19.
[28] Suresh S. Fatigue of materials. second ed. Cambridge: Cambridge University Press; 1998.
[29] Manigandana K, Srivatsan TS, Quick T. Influence of silicon carbide particulates on tensile fracture behavior of an aluminum alloy. Mater Sci Eng A 2012;534:711–5.
[30] Srivatsan TS, Lavernia EJ. Effects of microstructure on the strain-controlled fatigue failure behavior of an aluminum-alloy/ceramic-particle composite. Comp Sci Technol 1993;49:303–13.
[31] Tjong SC, Wang GS, Mai YW. Low-cycle fatigue behavior of Al-based composites containing in situ TiB_2, Al_2O_3 and Al_3Ti reinforcements. Mater Sci Eng A 2003;358:99–106.
[32] Ni DR, Chen DL, Xiao BL, Wang D, Ma ZY. Residual stresses and high cycle fatigue properties of friction stir welded SiCp/AA2009 composites. Int J Fatigue 2013;55:64–73.
[33] Ni DR, Chen DL, Wang D, Xiao BL, Ma ZY. Tensile properties and strain-hardening behaviour of friction stir welded SiCp/AA2009 composite joints. Mater Sci Eng A 2014;608:1–10.
[34] Styles MJ, Hutchinson CR, Chen Y, Deschamps A, Bastow TJ. The coexistence of two S (Al_2CuMg) phases in Al–Cu–Mg alloys. Acta Mater 2012;60:6940–51.
[35] Schueller RD, Sachdev AK, Wawner FE. Identification of a cubic precipitate observed in an Al–4.3Cu–2Mg SiC cast composite. Scr Metall Mater 1992;27:617–22.
[36] Ni DR, Chen DL, Wang D, Xiao BL, Ma ZY. Influence of microstructural evolution on tensile properties of friction stir welded joint of rolled SiCp/AA2009-T351 sheet. Mater Des 2013;51:199–205.
[37] Feng AH, Xiao BL, Ma ZY. Effect of microstructural evolution on mechanical properties of friction stir welded AA2009/SiCp composite. Comp Sci Technol 2008;68:2141–8.
[38] Rodrigo P, Poza P, Utrilla MV, Ureña A. Identification of σ and Ω phases in AA2009/SiC composites. J Alloys Compd 2009;482:187–95.
[39] Callister WD, Rethwisch DG. Materials science and engineering: an introduction. 9th ed. New York: John Wiley & Sons, Inc.; 2014. p. 637–9.
[40] Hollomon JH. Tensile deformation. Trans AIME 1945;162:268–90.
[41] Afrin N, Chen DL, Cao X, Jahazi M. Strain hardening behavior of a friction stir welded magnesium alloy. Scr Mater 2007;57(11):1004–7.
[42] Cho K, Gurland J. Law and mixtures applied to the plastics deformation of two-phase alloys of coarse microstructures. Metall Trans 1988;19A(8):2027–40.
[43] Nardone VC, Prewo KM. On the strength of discontinuous silicon carbide reinforced aluminum composites. Scr Metal 1986;20(1):43–8.
[44] Arsenault RJ, Wang L, Feng CR. Strengthening of composites due to microstructural changes in the matrix. Acta Metall Mater 1991;39(1):47–57.
[45] Zhang Q, Chen DL. A model for predicting the particle size dependence of the low cycle fatigue life in discontinuously reinforced MMCs. Scr Mater 2004;51(9):863–7.
[46] Zhang Z, Chen DL. Consideration of Orowan strengthening effect in particulate-reinforced metal matrix nanocomposites: a model for predicting their yield strength. Scr Mater 2006;54(7):1321–6.
[47] Zhang Q, Chen DL. A model for low cycle fatigue life prediction of discontinuously reinforced MMCs. Int J Fatigue 2005;27(4):417–27.
[48] Zhang Z, Chen DL. Contribution of Orowan strengthening effect in particulate-reinforced metal matrix nanocomposites. Mater Sci Eng A 2008;483–484:148–52.
[49] Dieter GE. Mechanical Metallurgy, McGraw-Hill Series. New York: McGraw-Hill; 1986.
[50] Chowdhury SH, Chen DL, Bhole SD, Powidajko E, Weckman DC, Zhou Y. Fiber laser welded AZ31 magnesium alloy: the effect of welding speed on microstructure and mechanical properties. Metall Mater Trans A 2012;43:2133–47.
[51] Mirza FA, Chen DL, Li DJ, Zeng XQ. Low cycle fatigue of a rare-earth containing extruded magnesium alloy. Mater Sci Eng A 2013;575:65–73.
[52] Christ HJ, Mughrabi H. Cyclic stress–strain response and microstructure under variable amplitude loading. Fatigue Fract Eng Mater Struct 1996;19(2/3):335–48.
[53] Jameel MA, Peralta P, Laird C. Masing behavior in copper single crystals fatigued under load Control. Mater Sci Eng A 2001;297:48–53.
[54] Niendorf T, Maier HJ, Canadinc D, Karaman I. On the cyclic stability and fatigue performance of ultrafine-grained interstitial-free steel under mean stress. Key Eng Mater 2008;378–379:39–52.